

## Level lifetimes in $^{32}\text{P}$ obtained using the Doppler-shift attenuation method with thick molecular targets

R. Bhattacharjee, S. S. Bhattacharjee, K. Basu, P. V. Rajesh, R. Raut,\* S. S. Ghugre, D. Das, and A. K. Sinha  
UGC-DAE Consortium for Scientific Research, Kolkata Centre, Kolkata 700098, India

L. Chaturvedi  
Guru Ghasidas University, Bilaspur 495009, India

U. Garg  
Department of Physics, University of Notre Dame, Notre Dame, Indiana 46556, USA

S. Ray  
Amity Institute of Nuclear Science and Technology, Amity University, Noida, Uttar Pradesh 201303, India

B. K. Yogi  
Department of Physics, Government College, Kota 324009, India

M. Kumar Raju  
Nuclear Physics Department, Andhra University, Visakhapatnam 530003, India

R. Chakrabarti and S. Mukhopadhyay  
Nuclear Physics Division, Bhabha Atomic Research Centre, Mumbai 400085, India

A. Dhal, R. P. Singh, N. Madhavan, and S. Muralithar  
Inter University Accelerator Centre, Aruna Asaf Ali Marg, New Delhi 110067, India

(Received 8 September 2014; revised manuscript received 22 September 2014; published 22 October 2014)

Level lifetimes in the  $^{32}\text{P}$  nucleus have been determined using the Doppler-shift attenuation method (DSAM). Conventional DSAM measurements employ a thin target on a thick, high- $Z$  backing. An extension of the technique to thick molecular targets is presented. The necessary modifications in the standard analysis procedures, pertaining to the incorporation of stopping power estimations for molecular media and evolution of residue cross section in a thick target, have been implemented. Further, x-ray powder diffraction (XRD) and scanning electron microscopy (SEM) have also been carried out to probe the structural composition of the target. The lifetime results have been validated with respect to the previous measurements and upper limits on lifetimes of seven levels have been determined for the first time. Large-basis shell model calculations have been carried out and compared with the experimental measurements.

DOI: [10.1103/PhysRevC.90.044319](https://doi.org/10.1103/PhysRevC.90.044319)

PACS number(s): 21.10.Tg, 21.10.Hw, 23.20.Lv, 27.30.+t

### I. INTRODUCTION

The high-spin states in nuclei in the vicinity of the island of inversion (interface of the  $sd$ - $fp$  orbitals), e.g.,  $^{26}\text{Mg}$ ,  $^{33}\text{S}$ , and  $^{32,33,34}\text{P}$ , have been the subjects of extensive experimental and theoretical investigations [1–6] in recent times. The low-lying positive parity states in these nuclei are expected to be dominated by pure  $sd$  configurations while the negative parity states involve excitations to the  $fp$  shell. Thus, the energy systematics of negative parity levels can be indicative of the evolution of the  $sd$ - $fp$  shell gap in the region. The level structure of some of these  $sdpf$  nuclei are well established experimentally providing a testing ground for large-basis spherical shell model calculations [2,7]. We have previously reported our spectroscopic investigation of the  $^{26}\text{Mg}$ ,  $^{32,33,34}\text{P}$ ,

and  $^{33}\text{S}$  [3,5,6], using heavy-ion induced fusion-evaporation reactions, wherein the level structures have been extended to higher spin domain. However, an unambiguous understanding of the structure requires information on the excited level lifetimes that helps us to identify the underlying microscopic configurations of the states. Herein we report the lifetime measurements for levels of the  $^{32}\text{P}$  nucleus, using the Doppler-shift attenuation method (DSAM) with a thick molecular target setup, along with a comparison with the shell model investigations.

The lifetimes of levels in  $^{32}\text{P}$ , below an excitation energy of 6.4 MeV, have been reported by Kangasmäki *et al.* [8] with due reference and comparison to the previous measurements (Table II of Ref. [8]). In the context of the present work, the lifetimes of the 1323, 1755, 3149, 3444, and 4276 keV levels are of importance. Of these states, only the lifetimes of the 1323 and the 1755 keV levels have been measured by Kangasmäki *et al.* while for the other three states the lifetimes have been

\*rraut@alpha.iuc.res.in

reanalyzed with respect to the previous measurements using the Monte Carlo approach. The 3149 keV state had previously been measured by Carr *et al.* [9] and Eijkern *et al.* [10] and the results from these measurements are in good agreement. The reevaluation of the 3149 keV level lifetime by Kangasmäki *et al.* complies with these reported values. The lifetime of the 3444 keV state had only been measured by Carr *et al.* [9] and the reanalysis by Kangasmäki *et al.* is in agreement with the measured value. The 3444 keV level with spin-parity  $J^\pi = 4^-$  is of particular importance since this is the lowest negative parity level and represents excitation to the  $pf$  shell in the  $^{32}\text{P}$  nucleus, from which an indication of the  $sd$ - $fp$  shell gap in the region can be obtained. The lifetime of the 4276 keV level had only been measured by Eijkern *et al.* [10] and the reanalysis by Kangasmäki *et al.* is in agreement, within the uncertainties, with the reported value. It is noteworthy that the aforesaid measurements of the lifetimes in the  $^{32}\text{P}$  nucleus have been carried out using modest experimental setups and may warrant a reexamination of these results in the light of contemporary facilities. In addition, our earlier reported spectroscopic investigation of the  $^{32}\text{P}$  nucleus [5] led to the observation of new levels, populated through heavy-ion induced fusion-evaporation reaction. Lifetime measurements for these levels are required to probe the underlying microscopic structure.

A wide range of experimental techniques are applied depending on the order of lifetime being measured. The Doppler-shift attenuation method (DSAM) is one of the commonly used techniques to measure lifetimes in the range of a few tens of femtoseconds ( $10^{-15}$  s) to a few picoseconds ( $10^{-12}$  s). The method is based on the observed Doppler effects as the recoiling nuclei, produced in a nuclear reaction, slow down (and eventually stop) within the target and/or the backing medium (stopping medium) while deexciting with the emission of  $\gamma$ -ray transitions. The Doppler effect consequently introduces either a shift or a broadening in the observed  $\gamma$ -ray energy, depending on both the level lifetime as well as the stopping time. The analysis of this observed shape/shift, with due incorporation of the slowing down of the recoils in the stopping medium and the time evolution of the level of interest (the formation time and its subsequent decay), facilitates the extraction of the level lifetimes. These measurements are performed at relatively large recoil velocities,  $\beta \geq 2\%$ , which results in a longer stopping time of the recoiling nuclei and makes the method sensitive to lifetimes typically in the aforementioned range.

Conventionally, the Doppler-shift attenuation method (DSAM) is carried out using a thin target, on a high- $Z$  elemental backing material. The choice of a thin target ensures that the energy loss of the recoiling nuclei occurs predominantly in a single medium, i.e., the backing medium. Further, the backing medium is chosen to be of elemental nature, reducing the uncertainties on the stopping simulations which, from the available experimental data, are better known for commonly used backing media such as gold, tantalum, lead, etc. The Doppler broadened  $\gamma$ -ray lineshapes are analyzed, for example, using the program LINESHAPE [11]. However, the code is primarily appropriate for the DSAM experiments carried out using a thin target along with a thick elemental

backing, and hence would require modifications to incorporate the alternative experimental scenarios as discussed herein.

The spectroscopic investigations of certain nuclei may require the use of a target which cannot be easily prepared in its pure elemental form. For example, the use of a neutron-rich target ( $^{18}\text{O}$ ) as well as a neutron-rich projectile ( $^{18}\text{O}$ ) could result in the population of high-spin states in nuclei at the interface of the  $sd$ - $fp$  orbitals. It is noteworthy that the  $^{18}\text{O}$  target can only be fabricated in a molecular form such as vanadium ( $\text{V}_2\text{O}_5$ ) or tantalum ( $\text{Ta}_2\text{O}_5$ ) pentoxide. Our group has reported the use of thick  $\text{Ta}_2\text{O}_5$  target, enriched in  $^{18}\text{O}$ , in the spectroscopic studies of these nuclei [3,5,6]. The Doppler lineshapes observed for the  $\gamma$ -ray transitions in these experiments cannot be analyzed within the purview of the standard LINESHAPE package. The present paper reports the modifications required to analyze the Doppler shapes obtained from thick molecular targets acting also as the stopping medium, validates the modifications with respect to the previously measured lifetimes in the  $^{32}\text{P}$  nucleus, extends the analysis to determine hitherto unknown lifetimes, and compares the results with the shell model calculations.

## II. EXPERIMENTAL DETAILS

The high spin states in  $^{32}\text{P}$  were populated using the  $^{18}\text{O}(^{16}\text{O},np)^{32}\text{P}$  reaction at an incident beam energy of 34 MeV. The details of the experimental setup are outlined in Ref. [3]. The neutron-rich  $^{18}\text{O}$  was prepared by heating a Ta foil of thickness  $\sim 50$  mg/cm<sup>2</sup>, in an enriched  $^{18}\text{O}$  atmosphere, resulting in the formation of  $\text{Ta}_2\text{O}_5$  on either side of the foil. The thickness of the  $\text{Ta}_2\text{O}_5$  on either side of the foil was estimated to be 9.25 mg/cm<sup>2</sup>. The deexciting  $\gamma$  rays were detected using the Indian National Gamma Array (INGA) [13], stationed at the 15 UD Pelletron Accelerator Centre at IUAC, New Delhi. The clover detectors of the INGA setup were placed at  $\theta = 32^\circ, 57^\circ, 90^\circ, 123^\circ,$  and  $148^\circ$  with respect to the beam axis. The energy calibration was carried out using radioactive sources as well as beam-off radioactivity data, which provided us with high-energy calibration points. The data were sorted in angle-dependent  $E_\gamma$ - $E_\gamma$  matrices with the  $90^\circ$  detectors on one axis and the detectors at one of the remaining angles on the other axis. The spectra demonstrating the Doppler effects (shapes) on the observed  $\gamma$  rays from the residual nuclei at forward and backward angles, with gates applied on coincident transitions at  $90^\circ$ , are illustrated in Fig. 1. The matrices were formed with energy dispersions of 0.5, 1, and 2 keV/channel, which were analyzed to ensure consistency of the extracted lifetimes. The observed  $\gamma$  ray at the five available angles were analyzed simultaneously (as detailed in the subsequent sections) for determination of the level lifetimes.

## III. PROGRAMMING MODIFICATIONS FOR DATA ANALYSIS

We report here the modifications in the LINESHAPE program [11] for the determination of the lifetimes of nuclear levels populated using a thick molecular target. The LINESHAPE

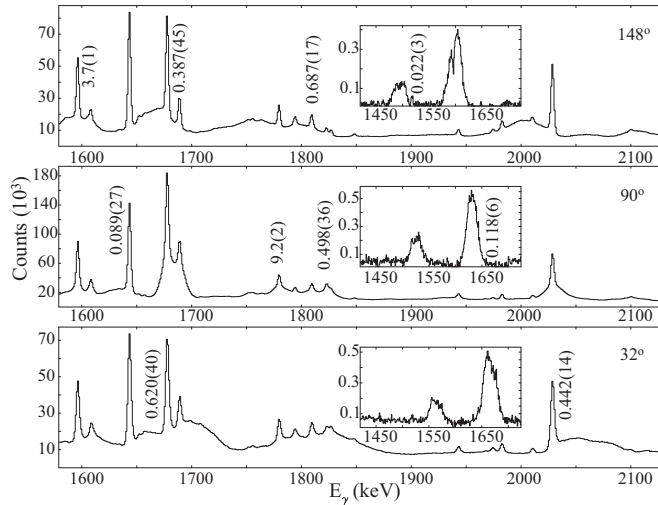


FIG. 1. Angle dependent projection spectra exhibiting Doppler effects on the  $\gamma$ -ray peaks observed in the present work. The labels indicate the reported lifetimes in ps [12]. The inset illustrates the Doppler shifted 1526 keV and 1631 keV (from  $^{29}\text{Si}$ ) peaks at forward and backward angles from very short lived levels.

program essentially consists of three major subprograms, as detailed below.

- (1) DECHIST simulates the velocity ( $\beta$ ) evolution of a given number of recoiling nuclei in the target and the backing media, using Monte Carlo techniques. It uses a set of stopping powers for the beam and the recoiling nuclei in the target and the backing media, that are computed using either (i) Ward's effective charge [14] and Ziegler's proton stopping powers [15] or (ii) Ziegler's heavy-ion stopping powers [15] or (iii) shell-corrected Northcliffe and Schilling stopping powers [16].
- (2) HISTAVER converts the time-dependent velocity histories of the recoiling nuclei into velocity profiles as viewed by the detectors at various angles.
- (3) LINESHAPE calculates the shapes for the  $\gamma$ -ray transitions of interest at different angles and performs a least-square fit of the experimentally observed shapes to determine the level lifetimes. The level lifetime ( $\tau$ ), side-feeding times ( $\tau_{sf}$ ), and spectrum parameters (such as centroid and background) are the parameters for the least-square fitting procedure.

The modifications in the LINESHAPE package have been carried out in the calculation of the stopping powers and incorporation of the cross-section dependence on the beam energy in the DECHIST program. These modifications are detailed herein.

### A. Stopping powers

The default prescription for computing the stopping power in the DECHIST program considers elemental medium only. A possible solution to include a compound medium would require using an *effective Z* and an *effective A* to approximate

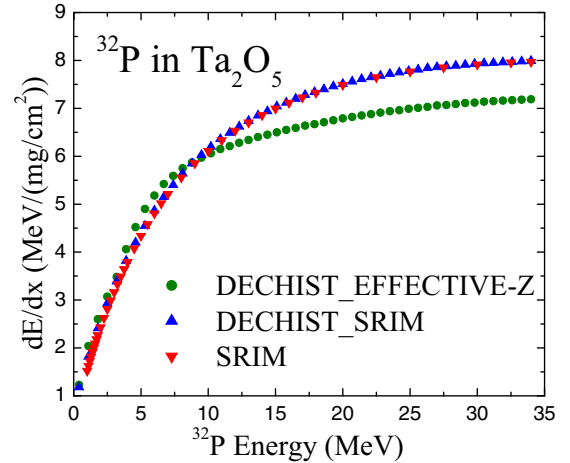


FIG. 2. (Color online) Stopping powers of  $^{32}\text{P}$  ions in  $\text{Ta}_2\text{O}_5$  using SRIM (labeled SRIM in the legend), DECHIST with SRIM input and interpolation (DECHIST\_SRIM) and DECHIST with effective  $Z$  and effective  $A$  for the  $\text{Ta}_2\text{O}_5$  target (DECHIST\_EFFECTIVE-Z).

the molecular media to an equivalent elemental form. The expressions used to calculate these quantities are as follows:

$$A_{\text{eff}} = \sum_i w_i A_i, \quad (1)$$

$$Z_{\text{eff}} = A_{\text{eff}} \sum_i \frac{Z_i w_i}{A_i} \quad (2)$$

where  $w_i$ ,  $A_i$ , and  $Z_i$  are respectively the weight or mass fraction of the species (element)  $i$ , its mass number, and its atomic number. Figure 2 illustrates the DECHIST calculated stopping power (labeled as DECHIST\_EFFECTIVE-Z) of  $\text{Ta}_2\text{O}_5$  medium for  $^{32}\text{P}$  ions, using  $Z_{\text{eff}} = 61$  and  $A_{\text{eff}} = 148$ .

Updated stopping powers for heavy ions in elemental as well as molecular media are available in contemporary software such as SRIM [17], and have been exhaustively benchmarked with respect to the experimental data and are considered to be more reliable. It would thus be appropriate to incorporate these stopping powers in the lifetime analysis. The stopping powers of  $^{32}\text{P}$  ions in  $\text{Ta}_2\text{O}_5$  from SRIM are included in Fig. 2. As is evident from the figure, the two approaches are approximately in agreement at lower energies, but deviate considerably in the higher energy domain, of kinematic relevance in the typical stopping calculations.

In the light of the reliability of the SRIM stopping powers, these have been incorporated in the modified DECHIST program and used in the current work. The DECHIST program calculates the stopping powers at 61 hard-coded energies, ranging from 1 keV to 1000 MeV, for the residue in the target and the backing, as well as for the beam in the target. The stopping powers required for all the intermediate energies are calculated through an in-built interpolation subroutine. The modified version of the program requires the user to provide these stopping powers, as calculated from SRIM (operating in batch mode), at these 61 energies through an input file. As already mentioned above, DECHIST calculates the stopping powers at relevant energies through interpolation. The interpolated

stopping powers for the  $^{32}\text{P} + \text{Ta}_2\text{O}_5$  case, as calculated by the modified DECHIST program, are also presented in the Fig. 2 (DECHIST\_SIRM). The overlap between the stopping powers calculated by SRIM and those calculated by DECHIST, with SRIM inputs and appropriate interpolation, validates the modification. A similar attempt to incorporate the SRIM calculated stopping powers in the LINESHAPE package has also been undertaken by Snyder *et al.* [18], though for an elemental medium.

### B. Cross-section dependence

A thin target ensures that the production cross section for the recoils, as a function of the beam energy, across the target can be assumed to be constant. Use of a thick target results in a substantial change (decrease) in the energy of the incident projectile as it traverses the target thickness and thus affects the production cross section of the residues along the depth of the target. Further, in a thick target, one needs to determine the thickness of the target that actually contributes to the residue production while the rest of the target thickness acts only as the stopping medium. The knowledge of target thickness contributing to the residue production follows from the information on the cross-section dependence on the beam energy and the evolution of the latter along the target thickness. The original version of the DECHIST program, that simulates the stopping of a given number of recoiling residues, divides the target thickness into bins equal to the (user) given number of recoil nuclei and treats each bin as the origin of one recoil nucleus. This is schematically represented in Fig. 3. As discussed above, this is a valid approximation for a thin target through which the beam energy can be assumed to remain unaltered and thus produce the residues with uniform probability (cross section).

In the modified version of the DECHIST program used in the present work, changes have been implemented to incorporate

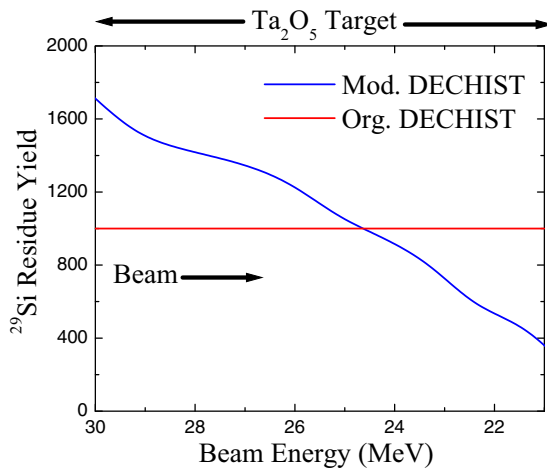


FIG. 3. (Color online) Cross-section of the residue as a function of beam energy. The original DECHIST program assigns a uniform cross section (red line) of the residue while the modified DECHIST program incorporates a beam-energy-dependent cross section (blue line) along the target thickness.

the cross-section dependence of the residues on the changing beam energy along the thickness of the target. In the present version of DECHIST, up to ten bins can be defined along the target thickness, and relative cross sections for the residue, in arbitrary units, can be specified therein, as illustrated in Fig. 3. The cross sections are preferably specified with reference to available experimental data or, in its absence, from statistical model calculations. It follows that the total thickness of the aforesaid bins is the thickness of the target that contributes in the production of the residues, while the remaining thickness contributes only in the stopping process. It is to be stressed that the knowledge of the target thickness contributing to the residue production emerges from the consideration of the energy dependence of the relevant cross section, and is imperative in the lifetime analysis in thick target setups.

It is understood that the aforesaid cross-section dependence on the changing beam energy would have a significant impact on the lifetime analysis of very-short-lived states, with  $\tau \sim$  tens of fs, exhibiting completely shifted peaks in the angular ( $\neq 90^\circ$ ) spectra. This is because the fast deexcitation following the short lifetime of the states occurs over a small fraction of the total stopping time, and thus is sensitive to the number of residues produced with a given recoil energy, an estimation of which comes from the cross-section considerations. The reaction  $^{18}\text{O}(^{16}\text{O},xnyp)$ , used in the present work, has also produced  $^{29}\text{Si}$  as one of the residues, with several short-lived levels (decaying with fast transitions) whose lifetimes have been previously reported. The Doppler shifts of the corresponding deexciting  $\gamma$ -ray peaks have been analyzed to demonstrate the effect of inclusion of the cross-section dependence. For instance, let us consider the 5254 keV level in the  $^{29}\text{Si}$  nucleus, deexciting by 1631 keV transition. The reported lifetime of the level is  $118 \pm 6$  fs [12]. The corresponding peak appears shifted in the forward and the backward angles, as illustrated in Fig. 1. The lifetime analysis, following the procedure detailed subsequently in the paper, has been carried out in the 1596 keV (bottom) gate. Owing to the side-feeding (sf) contribution in the bottom gate, only the upper limit ( $\tau_{\text{level}} + \tau_{\text{sf}}$ ) on the level lifetime could be obtained. The lifetime obtained without the inclusion of the cross-section effect is  $\tau \leq 74$  fs, which is distinctly discrepant with respect to the reported value. The corresponding fit is illustrated in Fig. 4. As already indicated before, ignoring the cross-section dependence implied that the residue could be produced within the entire thickness of the target ( $9.25 \text{ mg/cm}^2$ ). However, the statistical model calculations indicate that the production of  $^{29}\text{Si}$  occurs only up to a thickness of  $4.4 \text{ mg/cm}^2$ . The lifetime obtained using this thickness, with a uniform production cross section throughout, is  $\tau \leq 190$  fs. Further, if a cross-section-dependent binning within the thickness of  $4.4 \text{ mg/cm}^2$  is incorporated, the resulting lifetime is  $\tau \leq 169$  fs, which is in better conformity with the reported value. Moreover in the latter case, the quality of lineshape fit is substantially better than the fit obtained in the analysis with full target thickness of  $9.25 \text{ mg/cm}^2$ , as illustrated in Fig. 4. This exercise demonstrates the importance of including cross-section effects in DSAM analysis for thick-target experiments.

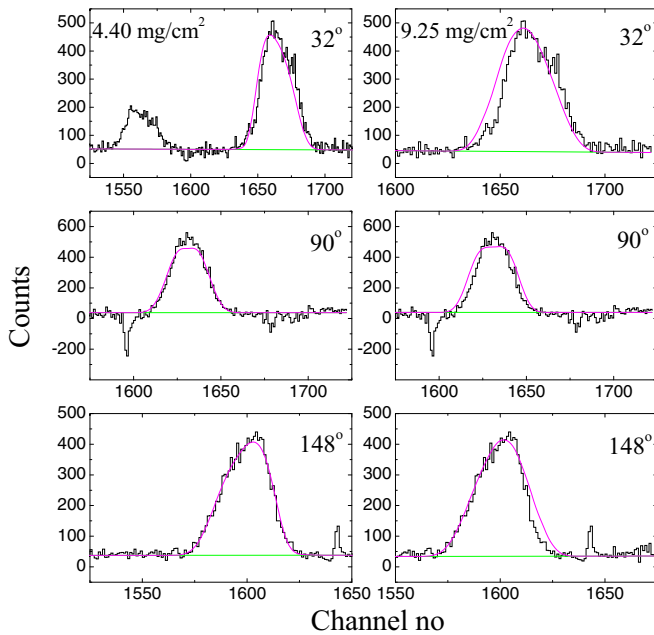


FIG. 4. (Color online) Least-square fitting of the 1631 keV peak from the  $^{29}\text{Si}$  nucleus, at  $32^\circ$ ,  $90^\circ$ , and  $148^\circ$ , using the LINESHAPE package. The peak exhibits Doppler shifts at forward and the backward angles. The fits correspond to the target thicknesses  $4.4 \text{ mg/cm}^2$  (effective) and  $9.25 \text{ mg/cm}^2$  (total), respectively.

#### IV. DENSITY CONSIDERATIONS IN OXIDE TARGETS

Most of the molecular targets used in nuclear spectroscopy experiments come in the form of oxides. It is possible that these oxides appear in several structural phases of varying density. The problem is further compounded if the targets are prepared through thermal oxidation which results in the formation of temperature-dependent oxidation states. The preparation may also lead to the formation of noncrystalline (amorphous) component. The consequent uncertainty pertaining to the structural composition of oxide targets can result in substantial discrepancies in the simulation of the stopping process and the lifetimes extracted therefrom. Thus, it is imperative to carry out a detailed investigation on the structural composition of the oxide target before concluding on the physical characteristics (density, etc.) that sensitively affect the slowing/stopping mechanism of the recoils in the target medium.

One of the effective tools to investigate the structural composition of the target is x-ray diffraction (XRD). The XRD measurements have been carried out for the  $\text{Ta}_2\text{O}_5$  target using a Bruker D8 Advance x-ray diffractometer. A copper source provided x rays of wavelength  $1.5418 \text{ \AA}$ . The spectrum has been acquired in  $\theta$ - $2\theta$  geometry with a step size of  $0.02^\circ$  in the range of  $5^\circ$  to  $70^\circ$ . The obtained diffraction pattern is presented in Fig. 5. The observed peaks have been assigned to both monoclinic and orthorhombic phases of crystalline  $\text{Ta}_2\text{O}_5$ . The inset of Fig. 5 shows a magnified view of the pattern in the range of  $10$  and  $25^\circ$ . The clear hump observed around  $12^\circ$  indicates presence of amorphous phase in the sample along with the crystalline phases.

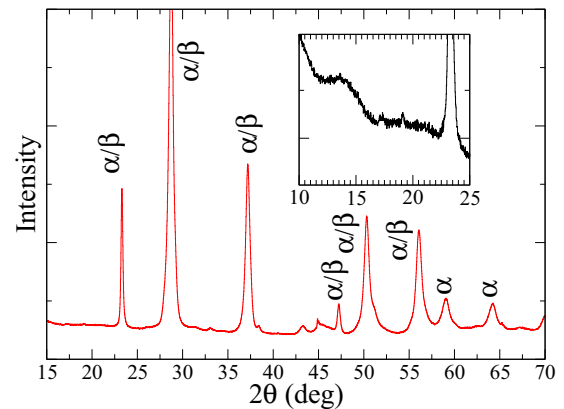


FIG. 5. (Color online) X-ray diffraction pattern obtained for  $\text{Ta}_2\text{O}_5$  target. The intensity scale is linear. The monoclinic and the orthorhombic phases of crystalline  $\text{Ta}_2\text{O}_5$  are identified by  $\alpha$  and  $\beta$  labels, respectively. The inset depicts the pattern at low angles. The observed hump at the low angles may be attributed to the presence of amorphous phase (see text).

The target has also been probed by field emission scanning electron microscopy (FESEM) using an INSPECT F50 scanning electron micrograph. A few selected micrographs are illustrated in Fig. 6. The upper panel shows a selected area of the target that confirms the polycrystalline nature of the target with a clear view of grain boundaries. The lower panel of Fig. 6 depicts white fluffy parts of the target confirming the presence of amorphous phase in the sample.

From the XRD and the SEM measurements it is thus concluded that the  $\text{Ta}_2\text{O}_5$  consists of both crystalline and amorphous phases. However, the quantification of the respective components is not feasible in the present case. The manifestation of the presence of these multiple phases in oxide targets could be a modification in the density of the target medium, a critical parameter in the stopping calculations. The effect of composite phases and components renders an ambiguity in the choice of the density parameter. This could be addressed if one considers a variation in the density to reproduce previously measured lifetimes.

As mentioned earlier, the detailed investigation of the level lifetimes of  $^{32}\text{P}$  by Kangasmäki *et al.* [8] justifies their use as calibration to determine the effective density of the  $\text{Ta}_2\text{O}_5$  target medium. The calculated density of  $\text{Ta}_2\text{O}_5$  from simple averaging of the elemental solid densities is  $5.76 \text{ g/cm}^3$  while the maximum theoretical density is  $8.2 \text{ g/cm}^3$ . The latter is also recorded in the compound database of the SRIM package. The lifetime of the  $1755 \text{ keV}$  ( $J_\pi = 3^+$ ) state in the  $^{32}\text{P}$  nucleus, deexciting by the  $1677 \text{ keV}$  transition, has been obtained (following the procedure detailed in the subsequent section) as a function of the density, and the corresponding plot is depicted in Fig. 7. As is evident from the figure, a density of  $5.76 \text{ g/cm}^3$  produces the best compliance with the reported lifetime for the state. This value has also been used in the lifetime analysis for the other nuclei populated in the same experiment, and the results are in agreement with the previously reported measurements. In the light of these results,

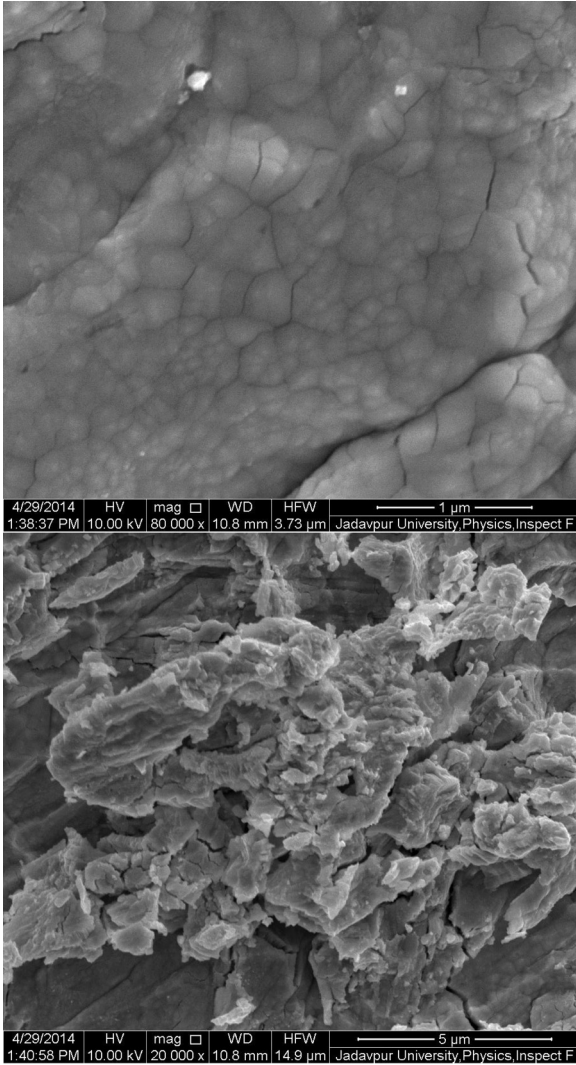


FIG. 6. Scanning electron micrograph images for  $\text{Ta}_2\text{O}_5$  target. The upper panel illustrates the crystalline component while the bottom panel indicates the presence of amorphous component.

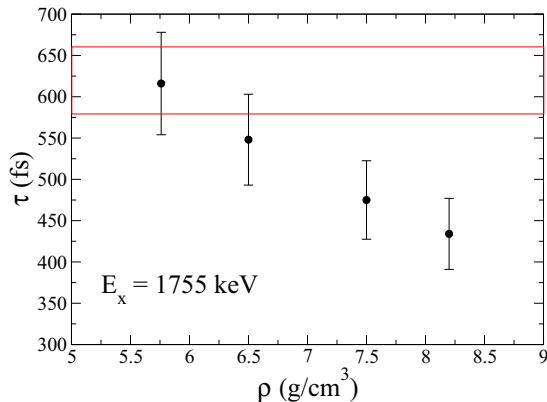


FIG. 7. (Color online) Variation of calculated lifetime for the 1755 keV state in the  $^{32}\text{P}$  nucleus as a function of the density of the  $\text{Ta}_2\text{O}_5$  target. The red band indicates the reported lifetime of the level along with the uncertainties.

this density has been used in all subsequent analysis reported in the present work.

It may be pointed out that, for  $\text{Ta}_2\text{O}_5$  in particular, it has been demonstrated by Martin *et al.* [19] that physical properties, such as density, are affected by the presence of microstructures originating from the fabrication methods which may justify the present empirical approach. Precedence for such methods has recently been reported by Peters *et al.* [20] for oxide targets.

## V. DATA ANALYSIS AND RESULTS

This section describes the procedure adopted in the present DSAM analysis along with the various parameters used to obtain the level lifetimes of the  $^{32}\text{P}$  nucleus. Monte Carlo simulation of the stopping process in the thick  $\text{Ta}_2\text{O}_5$  target has been carried out with the modified DECHIST program for 10 000 histories. Stopping powers used for the simulation have been obtained using the SRIM package. The cross section for the production of the  $^{32}\text{P}$  residue as a function of beam energy has been obtained from the statistical model calculations using the PACE4 code [21] and incorporated in the stopping calculations. A time step of 0.002 ps has been chosen for the simulation. The velocity profiles of the residual nuclei for detectors at  $148^\circ$ ,  $123^\circ$ ,  $90^\circ$ ,  $57^\circ$  and  $32^\circ$  have been individually calculated using the HISTAVER program.

The program LINESHAPE has been used to calculate the expected Doppler shape for a given  $\gamma$ -ray transition peak at a particular angle and perform a least-square fit to the corresponding experimental spectrum in order to extract the level lifetime ( $\tau$ ). The  $\gamma$ -ray spectra at five different angles have been fitted simultaneously for determination of the lifetime. The spectra have been generated with gates on transition either above (GTA) or below (GTB) the transition of interest, in the level scheme. In the case of the GTB procedure, the side-feeding is one of the crucial factors in the lifetime estimation and has been modeled in the present case with a single-step feeder level. The lifetime of this feeder level is a variable parameter in the least-square fitting process. It is understood that in the GTB procedure, due to contributions from a dominant side-feeding process, one can only estimate an upper limit of the level lifetime which is the sum of the level lifetime and the side-feeding time, resulting from the least-square fitting exercise. In contrast, the GTA technique, which eliminates the side-feeding contribution, is a more deterministic analysis resulting in the actual lifetime of the level of interest. However, often owing to the sparse statistics in the peak of interest, particularly in the high spin states populated in the heavy-ion-induced fusion-evaporation reaction, the GTA may have a limited scope in the lifetime analysis of the acquired data. The application of the GTA procedure in the present work is schematically represented in Fig. 8. Let us assume that L1 is the level of interest, deexcited by the  $\gamma_1$  transition. In the GTA technique, the L1 level lifetime has to be extracted from the  $\gamma_2$  gate (deexciting level L2). LSF is the side-feeder to L2. In the first step, the lifetime ( $\tau_2$ ) and the side-feeding time ( $\tau_{\text{SF}}$ ) of L2 are extracted from the lineshape analysis of the  $\gamma_2$  transition from the  $\gamma_1$  gated spectra. The lifetime of L2 ( $\tau_2$ ) and the corresponding side-feeding time ( $\tau_{\text{SF}}$ ) can be perceived as the feeding (formation) time

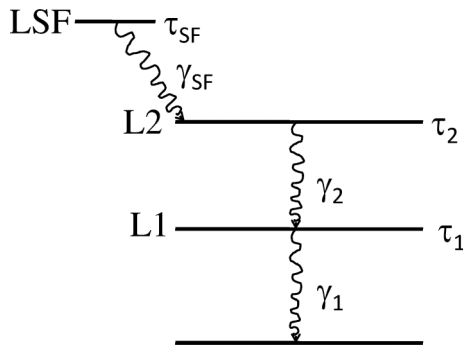


FIG. 8. Schematic representation of the gating from transition above (GTA) procedure for determination of the level lifetime, as applied in the present work (see text).

distribution of the level L1. In the second step of the analysis, the lifetime of L1 is determined from the lineshape analysis of the  $\gamma_1$  peak in the  $\gamma_2$  gated spectra, wherein the  $\tau_2$  and the  $\tau_{\text{SF}}$ , representing the feeding time distribution of L1, are provided as inputs and held fixed in the least-square fitting process. The least-square fitting parameters include those pertaining to the experimental spectrum such as the background, peak height, and the contaminant peaks. These parameters are initially varied in the minimization procedure but eventually held fixed, corresponding to the best fit, while determining the final value of the level lifetime. Chi-square analysis has been carried out to estimate the uncertainties on the level lifetimes. However, the principal uncertainties in the lifetime measurements originate from the errors pertaining to the estimation of the stopping powers used in the calculations. Typically, these uncertainties are known to be  $\sim 10\%$ . Thus, the stopping powers have been varied by  $\pm 10\%$  and the resulting dispersions in the level lifetimes have been included in the quoted uncertainties.

The lifetimes of the states in the  $^{32}\text{P}$  nucleus, derived from the present work, are summarized in Table I and the partial level scheme of the nucleus, illustrating the aforesaid levels, is depicted in Fig. 9. Representative fits to the observed lineshape are illustrated in Fig. 10. As included in Table I, lifetimes, or upper limits on the same, of 13 levels have been extracted from the present study. Of these, lifetimes for six states (1323, 1755, 3149, 3444, 4036, and 4276 keV) were previously known while an upper limit on those of the remaining seven states have been reported for the first time following the present investigation. Owing to the sparse statistics in the gated spectra, lifetimes of only a few levels could be determined by the GTA technique, while for the other levels the GTB procedure has been carried out. Consequently, only an upper limit on the corresponding level lifetime could be assigned.

The GTA technique could be carried out to determine the lifetimes of the levels at 1323 and 1755 keV. For the 1323 keV transition, the feeding time distribution, as defined earlier, has been determined by analyzing the lineshape of the 1826 keV transition in the 1323 keV gated spectra. This feeding time distribution has been kept fixed to determine the lifetime of the 1323 keV level, through least-square fitting of the Doppler shape of the 1323 keV peak, in the 1826 keV gated spectra. The lifetime of the 1323 keV level has also been determined from

TABLE I. Lifetimes of the states in  $^{32}\text{P}$  from the present work in comparison to the previously reported values. The quoted uncertainties include the effect of the uncertainties in the stopping powers. Please refer to the text for details.

| $J_i^\pi$   | $E_x$<br>(keV)    | $E_\gamma$<br>(keV) | $\tau$ (fs)           |                     |
|-------------|-------------------|---------------------|-----------------------|---------------------|
|             |                   |                     | Present work          | NNDC                |
| $2_2^+$     | 1323              | 1323                | $485^{+57}_{-32}$     | $488^{+25}_{-25}$   |
|             |                   | 1245                | $472^{+38}_{-23}$     |                     |
| $3_1^+$     | 1755              | 1677                | $616^{+65}_{-46}$     | $620^{+40}_{-40}$   |
| $4_1^+$     | 3149              | 1826                | $<745^{+83a}_{-76}$   | $498^{+36}_{-36}$   |
| $4_1^-$     | 3444              | 1689                | $<883^{+103a}_{-82}$  | $387^{+45}_{-45}$   |
| $4_2^+$     | 4036              | 2281                | $<80^{+22a}_{-10}$    | $35^{+25}_{-25}$    |
| $5_1^-$     | 4276              | 1127                | $<696^{+99a}_{-42}$   | $779^{+115}_{-115}$ |
|             |                   | 832                 | $<902^{+85a}_{-101}$  |                     |
|             | 4698              | 1254                | $<579^{+69a}_{-62}$   |                     |
| $5_2^{(-)}$ | 5481 <sup>b</sup> | 2037                | $<188^{+36a}_{-29}$   |                     |
| $6_1^{(-)}$ | 5862 <sup>b</sup> | 2418                | $<629^{+82a}_{-61}$   |                     |
|             |                   | 6415 <sup>b</sup>   | $<186^{+30a}_{-30}$   |                     |
|             | 6835 <sup>b</sup> | 2559                | $<159^{+30a}_{-23}$   |                     |
| $7^{(-)}$   | 7417 <sup>b</sup> | 1555                | $<1018^{+130a}_{-82}$ |                     |
| $(8^-)$     | 9637 <sup>b</sup> | 2220                | $<220^{+30a}_{-27}$   |                     |

<sup>a</sup>The presence of a dominant side-feeding allowed for assignment of only an upper limit on the lifetime.

<sup>b</sup>New level, first reported in our earlier work [5].

the Doppler shape analysis of the 1245 keV peak, observed in the 1826 keV gate. The lifetime of the level results from the analysis of the two individual transitions which are in excellent agreement, as recorded in Table I, and it is in compliance with the previously reported lifetime for the level. As far as the lifetime analysis of the 1755 keV level is concerned, feeding time distribution has been extracted from the analysis of the lineshape of the 1689 keV transition observed in the 1677 keV gated spectra. This distribution has been used in the lifetime analysis of the 1755 keV level in the 1689 keV gated spectra. The lifetime (616 fs) obtained therefrom is in excellent overlap with the previously reported value (620 fs). This exercise demonstrates the feasibility of undertaking DSAM analysis on data acquired from thick molecular targets.

Upper limits on the lifetimes of the remaining levels have been obtained from the GTB procedure and are included in Table I.

The experimental level lifetimes, obtained from the present analysis, are compared with those from large-basis shell model calculations, as detailed in the next section.

## VI. SHELL MODEL CALCULATIONS

Nuclei at the interface of  $sd$ - $fp$  shells have been extensively probed within the framework of large-basis shell model calculations [2,7]. Lifetime measurements provide stringent testing grounds for these theoretical calculations, in particular

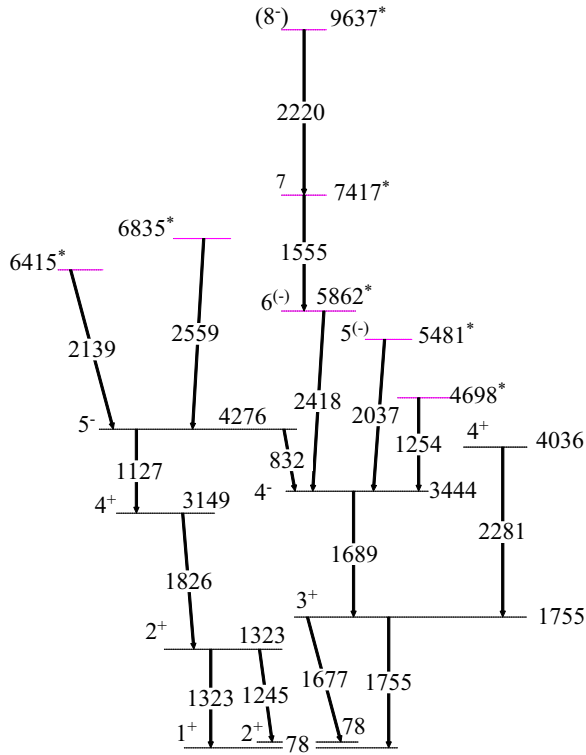


FIG. 9. (Color online) Partial level scheme of  $^{32}\text{P}$  illustrating levels whose lifetimes have been measured in the present work. The lifetimes of the levels marked \* have been measured for the first time in the present investigation.

for the validation of the two-body interactions. In recent times there have been developments of new interactions for these nuclei, that incorporates the contemporary experimental findings [2,7,22]. In the present work, large-basis shell model calculations for the  $^{32}\text{P}$  nucleus have been carried out. Lifetime results obtained from the present experiment as well as from the previous studies have been compared with the model predictions. The shell model code NUSHELLX@MSU [23] has been used for the purpose, wherein different model spaces and interactions have been used for a comprehensive comparison.

The positive parity states have been calculated using the  $sd$  model space, consisting of the  $1d_{5/2}, 2s_{1/2}, 1d_{3/2}$  orbitals, and with the USDA interaction. The effective nucleon charges used are  $e_p = 1.36$  and  $e_n = 0.45$  [2]. The results are summarized in Table II. The calculated lifetime of the 1323, 1755, 3149 keV states, are in excellent agreement with the measurements.

The negative parity states essentially originate from the  $1p-1h$  excitations into the  $fp$  shell. These have been calculated using the  $sdpf$  model space, consisting of the  $1d_{5/2}, 2s_{1/2}, 1d_{3/2}$  and  $1f_{7/2}, 2p_{3/2}, 2p_{1/2}, 1f_{5/2}$  orbitals, along with the  $sdpfmw$  and the  $sdpflu$  interactions. The effective nucleon charges used are, identical to the USDA interaction,  $e_p = 1.36$  and  $e_n = 0.45$ . A truncation scheme has been implemented, allowing a maximum of one neutron particle in the  $fp$  shell, either in the  $1f_{7/2}$  or in the  $2p_{3/2}$  orbital. This was necessitated owing to the fact that the calculations with the

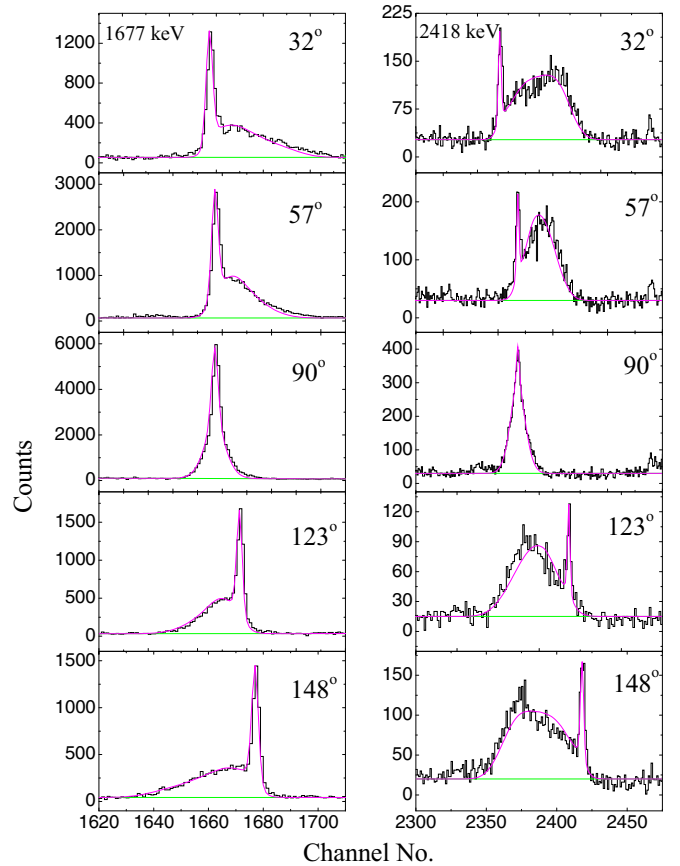


FIG. 10. (Color online) Representative fits of the Doppler shapes of the 1677 and 2418 keV transitions from the  $^{32}\text{P}$  nucleus, obtained in the present work.

full  $fp$  shell resulted in considerable lowering of the predicted excitation energies. The results (level energies and lifetimes) of the model calculations in comparison to the experimental findings are recorded in Table II. The experimental transition probabilities [ $B(M1)$ ,  $B(E2)$ ] and the branching ratios are compared with the shell model predictions in Table III. Results for the 3<sup>-</sup> and 4<sup>-</sup> states, that decay by  $E1$  transitions, could not be compared with the shell model calculations. The calculations are in general agreement with the experimental results. The deviations between the experimental and the calculated quantities, particularly for the negative parity states, may warrant reevaluation of the two-body matrix elements in this region.

## VII. CONCLUSION

Lifetimes of the excited states in the  $^{32}\text{P}$  nucleus have been measured using the DSAM technique, carried out with thick molecular targets. The extended analysis procedure has been validated with respect to the previously reported measurements. Upper limits on lifetimes of the levels  $E_x = 4698, 5481, 5862, 6415, 6835, 7417$  and,  $9637$  keV in the nucleus have been determined for the first time. Experimental results have been compared with the shell model calculations for states for which the spin-parity assignments were



TABLE II. Comparison of experimental and shell model calculated level energies and lifetimes in  $^{32}\text{P}$ . The states with lifetimes measured in the present work have been marked in bold font.

| $E_x$<br>(keV) | $J^\pi$     | $\tau$                                    |                                 | Shell model calculation |                |                |                |                |                |
|----------------|-------------|---|---------------------------------|-------------------------|----------------|----------------|----------------|----------------|----------------|
|                |             | This work<br>(fs)                         | NNDC<br>(fs)                    | USDA                    |                | SDPFMW         |                | SDPFMU         |                |
|                |             |   |                                 | $E_x$<br>(keV)          | $\tau$<br>(fs) | $E_x$<br>(keV) | $\tau$<br>(fs) | $E_x$<br>(keV) | $\tau$<br>(fs) |
| 0              | $1_1^+$     |   |                                 | 0                       | 0              | 6              |                | 0              |                |
| 78             | $2_1^+$     |   |                                 | 177                     | 60280          | 0              |                | 4              |                |
| 513            | $0_1^+$     |   | $2641 \pm 115$                  | 646                     | 4355           | 260            | 17988          | 216            | 39221          |
| 1149           | $1_2^+$     |   | $264 \pm 17$                    | 1030                    | 616            | 1048           | 154            | 1109           | 102            |
| <b>1323</b>    | $2_2^+$     | <b><math>485^{+57}_{-32}</math></b>       | <b><math>488 \pm 25</math></b>  | <b>1291</b>             | <b>487</b>     | <b>1135</b>    | <b>2941</b>    | <b>1162</b>    | <b>2181</b>    |
| <b>1755</b>    | $3_1^+$     | <b><math>616^{+65}_{-46}</math></b>       | <b><math>620 \pm 40</math></b>  | <b>1832</b>             | <b>729</b>     | <b>1528</b>    | <b>1215</b>    | <b>1595</b>    | <b>854</b>     |
| 2177           | $3_2^+$     |   | $76 \pm 14$                     | 2292                    | 36             | 2225           | 54             | 2309           | 49             |
| 2218           | $2_3^+$     |   | $240 \pm 25$                    | 2314                    | 124            | 2037           | 101            | 2175           | 46             |
| 2658           | $2_4^+$     |   | $12 \pm 4$                      | 2594                    | 10.5           | 2602           | 10             | 2570           | 10             |
| <b>3149</b>    | $4_1^+$     | <b><math>&lt;745^{+83}_{-76}</math></b>   | <b><math>498 \pm 36</math></b>  | <b>3219</b>             | <b>370</b>     | <b>3168</b>    | <b>124</b>     | <b>3132</b>    | <b>131</b>     |
| <b>4036</b>    | $4_2^+$     | <b><math>&lt;80^{+22}_{-10}</math></b>    | <b><math>35 \pm 25</math></b>   | <b>4119</b>             | <b>10.3</b>    | <b>3727</b>    | <b>12</b>      | <b>3857</b>    | <b>10</b>      |
| <b>4276</b>    | $5_1^-$     | <b><math>&lt;902^{+85}_{-101}</math></b>  | <b><math>779 \pm 115</math></b> |                         |                | <b>4106</b>    | <b>927</b>     | <b>3576</b>    | <b>1257</b>    |
| <b>5481</b>    | $5_2^{(-)}$ | <b><math>&lt;188^{+36}_{-29}</math></b>   |                                 |                         |                | <b>5358</b>    |                | <b>4886</b>    |                |
| <b>5862</b>    | $6_1^{(-)}$ | <b><math>&lt;629^{+82}_{-61}</math></b>   |                                 |                         |                | <b>5640</b>    | <b>190</b>     | <b>5136</b>    | <b>250</b>     |
| <b>7417</b>    | $7_1^{(-)}$ | <b><math>&lt;1018^{+130}_{-82}</math></b> |                                 |                         |                | <b>6846</b>    | <b>80</b>      | <b>6189</b>    | <b>108</b>     |
| <b>9637</b>    | $(8_1^-)$   | <b><math>&lt;220^{+30}_{-27}</math></b>   |                                 |                         |                | <b>8834</b>    | <b>127</b>     | <b>8009</b>    | <b>213</b>     |

known from earlier studies. The positive parity states have been successfully interpreted using the USDA interaction. The cross shell calculations using the *sdpfmw* and the *sdpfmu* interactions for the negative parity states exhibit

comparable results, which are in satisfactory agreement with the experimental observations. The presence of transitions with  $\tau \sim 200$  fs around  $E_x \sim 6$  MeV may indicate the possible onset of collectivity and warrants the necessity of

TABLE III. Comparison of the experimental transition probabilities and branching ratios, wherever possible, with those from the shell model calculations. The assignments (M) are quoted from NNDC [12] and/or previous work [5].

| $E_x$<br>(keV) | $E_\gamma$<br>(keV) | M                | Experimental              |                                 |                   | Shell model              |                                 |       |                          |                                 |        |                          |                                 |      |
|----------------|---------------------|------------------|---------------------------|---------------------------------|-------------------|--------------------------|---------------------------------|-------|--------------------------|---------------------------------|--------|--------------------------|---------------------------------|------|
|                |                     |                  | $B(M1)$<br>( $\mu_n^2$ )  | $B(E2)$<br>( $e^2\text{fm}^4$ ) | BR                | USDA                     |                                 |       | SDPFMW                   |                                 |        | SDPFMU                   |                                 |      |
|                |                     |                  |                           |                                 |                   | $B(M1)$<br>( $\mu_n^2$ ) | $B(E2)$<br>( $e^2\text{fm}^4$ ) | BR    | $B(M1)$<br>( $\mu_n^2$ ) | $B(E2)$<br>( $e^2\text{fm}^4$ ) | BR     | $B(M1)$<br>( $\mu_n^2$ ) | $B(E2)$<br>( $e^2\text{fm}^4$ ) | BR   |
| 1323           | 1323                | <i>M1</i>        | $0.027^{+0.002}_{-0.003}$ |                                 | $0.53 \pm 0.01$   | 0.041                    | 0.68                            | 0.007 | 0.71                     | 0.008                           | 0.63   |                          |                                 |      |
|                | 1245                | <i>M1</i>        | $0.029^{+0.002}_{-0.003}$ |                                 | $0.47 \pm 0.01$   | 0.031                    | 0.32                            | 0.002 | 0.25                     | 0.004                           | 0.31   |                          |                                 |      |
| 1755           | 1755                | <i>E2 + M3</i>   |                           | $0.796^{+0.076}_{-0.064}$       | $0.010 \pm 0.001$ |                          | 0.782                           | 0.02  | 0.033                    | 0.00                            | 0.398  | 0.00                     |                                 |      |
|                | 1677                | <i>M1 + E2</i>   | $0.012^{+0.001}_{-0.001}$ | $37.611^{+3.035}_{-3.590}$      | $0.98 \pm 0.02$   | 0.001                    | 50.490                          | 0.86  | 0.003                    | 56.010                          | 0.94   | 0.006                    | 66.160                          | 0.96 |
|                | 432                 | <i>M1 + E2</i>   | $0.022^{+0.002}_{-0.002}$ | $24.980^{+2.033}_{-2.370}$      | $0.020 \pm 0.001$ | 0.027                    | 0.327                           | 0.11  | 0.043                    | 0.395                           | 0.05   | 0.032                    | 0.348                           | 0.03 |
| 3149           | 3071                | <i>E2 + M3</i>   |                           | $0.299^{+0.024}_{-0.020}$       | $0.050 \pm 0.004$ |                          | 0.571                           | 0.07  | 3.164                    | 0.15                            | 5.096  | 0.22                     |                                 |      |
|                | 1826                | <i>E2 + M3</i>   |                           | $44.980^{+3.032}_{-3.505}$      | $0.56 \pm 0.02$   |                          | 50.460                          | 0.73  | 34.97                    | 0.18                            | 44.980 | 0.20                     |                                 |      |
|                | 1394                | <i>M1 + E2</i>   | 0.000                     | $41.766^{+3.255}_{-2.816}$      | $0.14 \pm 0.01$   | 0.002                    | 46.880                          | 0.14  | 0.056                    | 50.74                           | 0.63   | 0.061                    | 60.840                          | 0.54 |
|                | 972                 | <i>M1 + E2</i>   | $0.031^{+0.002}_{-0.002}$ | $5.645^{+0.439}_{-0.381}$       | $0.25 \pm 0.01$   | 0.011                    | 5.370                           | 0.06  | 0.018                    | 4.79                            | 0.03   | 0.030                    | 2.343                           | 0.04 |
| 4036           | 2281                | <i>M1 + (E2)</i> | $0.137^{+0.342}_{-0.069}$ |                                 | 1.00              | 0.267                    | 9.583                           | 0.59  | 0.303                    | 3.609                           | 0.68   | 0.328                    | 3.270                           | 0.63 |
| 4276           | 832                 | <i>M1 + E2</i>   | $0.096^{+0.016}_{-0.013}$ | $38.890^{+6.737}_{-5.001}$      | $0.77 \pm 0.12$   |                          |                                 |       | 0.076                    | 8.783                           | 0.95   | 0.094                    | 11.380                          | 0.99 |
| 5862           | 1586                | ( <i>M1</i> )    | $>0.001$                  |                                 | $0.030 \pm 0.002$ |                          |                                 |       | 0.004                    |                                 | 0.05   | 0.011                    |                                 | 0.18 |
|                | 2418                | <i>E2 + M3</i>   |                           | $>13.986$                       | $0.89 \pm 0.02$   |                          |                                 |       |                          | 46.700                          | 0.95   |                          | 37.770                          | 0.81 |

further investigation. This work demonstrates the feasibility of undertaking DSA measurements using a molecular target, thus extending the scope of the technique. However, understanding of the structural composition and the stopping characteristics of the target medium have been identified to remain as the essential inputs in such endeavors.

### ACKNOWLEDGMENTS

The authors thank all the participants of the INGA collaboration for their help in setting up the facility at IUAC, New Delhi. We are thankful to J. P. Greene (ANL, USA) for the  $^{18}\text{O}$  target. We thank the Pelletron staff at IUAC, New Delhi

for their excellent support during the experiment. Discussions with Prof. Alex Brown on the shell model calculations have been of much help and are deeply appreciated. The help in SEM measurements received from Dr. S. Kumar and Dr. S. Das of the Department of Physics, Jadavpur University is gratefully acknowledged. The SEM facility at the Department of Physics, Jadavpur University is supported by the Department of Science and Technology (DST), Government of India, under the FIST Program. S.S.B. would like to acknowledge financial assistance in the form of a fellowship [SRF, CSIR sanction No. 09/838(0038)2010-EMR-I] from the Council of Scientific and Industrial Research (CSIR), Government of India. The INGA Project is partially supported by the DST under Grant No. IR/S2/PF-03/2003-III.

- 
- [1] B. A. Brown and B. H. Wildenthal, *Annu. Rev. Nucl. Part. Sci.* **38**, 29 (1988).
- [2] W. A. Richter, S. Mkhize, and B. A. Brown, *Phys. Rev. C* **78**, 064302 (2008).
- [3] R. Chakrabarti, S. Mukhopadhyay, Krishichayan, A. Chakraborty, A. Ghosh, S. Ray, S. S. Ghugre, A. K. Sinha, L. Chaturvedi, A. Y. Deo *et al.*, *Phys. Rev. C* **80**, 034326 (2009).
- [4] P. C. Bender, C. R. Hoffman, M. Wiedeking, J. M. Allmond, L. A. Bernstein, J. T. Burke, D. L. Bleuel, R. M. Clark, P. Fallon, B. L. Goldblum *et al.*, *Phys. Rev. C* **80**, 014302 (2009).
- [5] R. Chakrabarti, S. Mukhopadhyay, R. Bhattacharjee, S. S. Ghugre, A. K. Sinha, A. Dhal, L. Chaturvedi, M. K. Raju, N. Madhavan, R. P. Singh *et al.*, *Phys. Rev. C* **84**, 054325 (2011).
- [6] S. S. Bhattacharjee, R. Bhattacharjee, R. Chakrabarti, R. Raut, S. S. Ghugre, A. K. Sinha, T. Trivedi, L. Chaturvedi, S. Saha, J. Sethi *et al.*, *Phys. Rev. C* **89**, 024324 (2014).
- [7] W. A. Richter and B. A. Brown, *Phys. Rev. C* **80**, 034301 (2009).
- [8] A. Kangasmäki, P. Tikkanen, J. Keinonen, W. E. Ormand, and S. Raman, *Phys. Rev. C* **55**, 1697 (1997).
- [9] P. E. Carr, D. C. Bailey, L. L. Green, A. N. James, J. F. Sharpey-Schafer, and D. A. Viggars, *J. Phys. A* **6**, 705 (1973).
- [10] F. E. H. van Eijkern, G. V. Middelkoop, J. Timmer, and J. A. van Luijk, *Nucl. Phys. A* **210**, 38 (1973).
- [11] J. C. Wells and N. R. Johnson, ORNL Report No. 6689, 1991, (unpublished), p. 44.
- [12] [www.nndc.bnl.gov](http://www.nndc.bnl.gov)
- [13] S. Muralithar, K. Rani, R. Kumar, R. P. Singh, J. J. Das, J. Gehlot, K. S. Golda, A. Jhingan, N. Madhavan, S. Nath *et al.*, *Nucl. Instrum. Methods Phys. Res. A* **622**, 281 (2010).
- [14] D. Ward, AECL Report No. 5313, 1976 (unpublished).
- [15] J. F. Ziegler, *The Stopping and Ranges of Ions in Matter* (Pergamon, Oxford, 1980).
- [16] L. C. Northcliffe and R. F. Schilling, *At. Data Nucl. Data Tables* **7**, 233 (1970).
- [17] [www.srim.org](http://www.srim.org)
- [18] J. B. Snyder, Ph.D. thesis, Washington University, 2013 (unpublished).
- [19] P. J. Martin, A. Bendavid, M. Swain, R. P. Netterfield, T. J. Kinder, W. G. Sainty, D. Drage, and L. Wielunski, *Thin Solid Films* **239**, 181 (1994).
- [20] E. E. Peters, A. Chakraborty, B. P. Crider, B. H. Davis, M. K. Gnanamani, M. T. McEllistrem, F. M. Prados-Estévez, J. R. Vanhoy, and S. W. Yates, *Phys. Rev. C* **88**, 024317 (2013).
- [21] A. Gavron, *Phys. Rev. C* **21**, 230 (1980).
- [22] F. Nowacki and A. Poves, *Phys. Rev. C* **79**, 014310 (2009).
- [23] B. A. Brown and W. D. M. Rae, MSU-NSCL report, 2007 (unpublished).